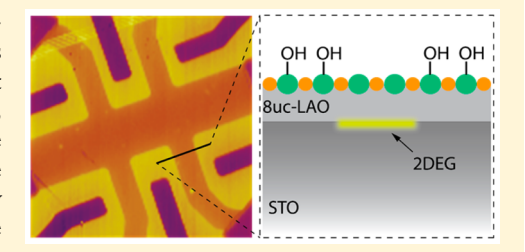


Tailoring LaAlO₃/SrTiO₃ Interface Metallicity by Oxygen Surface **Adsorbates**

Weitao Dai,[†] Sanjay Adhikari,[†] Andrés Camilo Garcia-Castro,^{‡,§} Aldo H. Romero,[†] Hyungwoo Lee,^{||} Jung-Woo Lee,^{||} Sangwoo Ryu,^{||} Chang-Beom Eom,^{||} and Cheng Cen^{*,†}

Supporting Information

ABSTRACT: We report an oxygen surface adsorbates induced metalinsulator transition at the LaAlO₃/SrTiO₃ interfaces. The observed effects were attributed to the terminations of surface Al sites and the resultant electron-accepting surface states. By controlling the local oxygen adsorptions, we successfully demonstrated the nondestructive patterning of the interface two-dimensional electron gas (2DEG). The obtained 2DEG structures are stable in air and also robust against general solvent treatments. This study provides new insights into the metal-insulator transition mechanism at the complex oxide interfaces and also a highly efficient technique for tailoring the interface properties.



KEYWORDS: 2DEG, oxide interfaces, adsorbates, charge transfer doping, surface states

he multifunctional characters^{1–14} of the two-dimensional electron gas (2DEG) formed at the interfaces between LaAlO₃ (LAO) and SrTiO₃ (STO)^{15,16} have made this material system a continuingly active field of research. A model involving the charge redistribution driven by the polar field in the LAO layer ("polar catastrophe") explained the critical LAO thickness (4 unit cell (uc)) required for the 2DEG formation. 17,18 Effects of defects, 19,20 cation-intermixing, 21,22 strain, 23 surface dangling bonds, 24 and multisubband transport 25,26 were also reported. The interplay between these different mechanisms adds to the complexity and richness of physics found in LAO/STO heterostructures.

Using surface related techniques to control the interface 2DEG is particularly appealing in LAO/STO systems. This is not only due to the surface's availability for engineering, but also because of the LAO surface's large electrostatic potential that can trigger the electrons redistribution. Different capping layers have been explored to control the built-in polar field or the defect level in oxide layers.^{27–31} The effects of surface adsorbates were also revealed by conducting atomic force microscopy (c-AFM) based experiments in samples with LAO layer thicknesses just below the critical value. 11,32-35 However, such effects are often considered secondary and only explicitly observable when the system is already near the metal-insulator transition point under the influence of polar catastrophe.

Here, we show that surface adsorbates can affect the interface doping as significantly as the polar catastrophe effect. Adding oxygen-related adsorbates to the LAO surface using oxygen plasma, the interfaces of samples with much thicker than 4 uc LAO layers can be transformed to a completely insulating state. Tuning of the interface doping level was achieved by controlling the oxygen plasma dosage. We also demonstrated the spatial patterning of the interface 2DEG by combining oxygen plasma surface treatment with commonly available lithography techniques. The simplicity of this very clean patterning method has clear advantages comparing to other approaches that were reported.^{36–38} The effects of oxygen adsorbates were jointly evaluated by scanning probe based surface characterizations and density functional theory (DFT) calculations. The results revealed a charge transfer mechanism that is critically influenced by extrinsic donors and electrontrapping states formed at the surface.

Figure 1 illustrates the evolvement of the interface 2DEG during and after two consecutive oxygen plasma exposures of identical dosage (300 W radio frequency (RF) power for 1.5 min). Generated by RF excitations, a large density of oxygen based negative ions (O-, O2-, O3-, etc.) were driven to the sample surface by a small electrical bias. Besides removing organic contaminants, oxygen plasma's effects in surface oxidation³⁹⁻⁴¹ and hydroxylation⁴²⁻⁴⁴ are also well known. Due to the low ion energies, oxygen plasma reacted only with the surface atoms. The most important reaction between the oxygen plasma and the LAO surface is expected to be the

Received: January 31, 2016 Revised: February 22, 2016 Published: March 1, 2016



Department of Physics and Astronomy, West Virginia University, Morgantown, West Virginia 26506, United States

[‡]Physique Théorique des Matériaux, Université de Liège, B-4000 Sart-Tilman, Belgium

[§]Centro de Investigación y Estudios Avanzados del IPN, MX-76230 Querétaro, México

Department of Material Science and Engineering, University of Wisconsin—Madison, Madison, Wisconsin 53706, United States

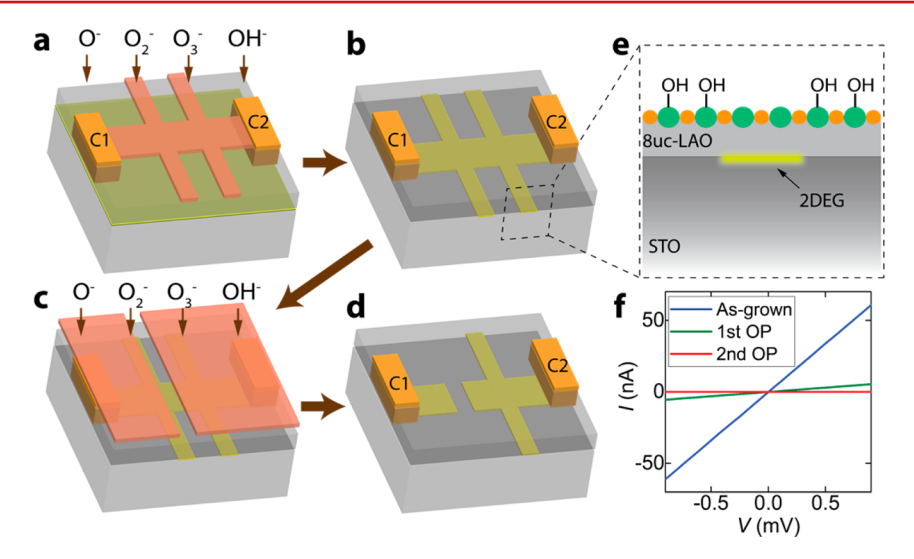


Figure 1. Patterning of interface 2DEG by oxygen plasma. (a-d) Illustrations of the two consecutive oxygen plasma exposures and the evolvement of interface 2DEG patterns. During the first (a) and second (c) exposures, different photoresist patterns (pink) were used to protect partial surface regions. (e) Illustration of the OH termination of surface Al sites when LAO surface is exposed to the ions in oxygen plasma. Orange circles indicate O atoms and green circles indicate Al atoms. Underneath the exposed surface regions, interface 2DEG is suppressed. (f) I-V curves measured between contacts C1 and C2 before and after the two oxygen plasma treatments.

termination of the surface Al sites by O or more stable OH after air exposure (Figure 1e).

As grown, the 8 uc LAO/STO sample had a planarconducting interface. I-V measurements between two interface contacts C1 and C2 yielded an initial resistance of 15 $k\Omega$ (Figure 1f, blue). A Hall bar shape AZ5214 photoresist layer was then patterned by photolithography to shield the underneath LAO surface during the first oxygen plasma treatment (Figure 1a). After the plasma exposure and resist removal, resistance between C1 and C2 increased to 166 k Ω (Figure 1f, green). The ratio of the resistance change is consistent with numerical simulations performed comparing a planar conducting interface and an interface that is insulating everywhere else except for the hall bar region (Supporting Information) (Figure 1b). This observation thus points to a room temperature metal-to-insulator transition in the regions exposed to oxygen plasma. To verify this effect more definitively, we performed the second oxygen plasma treatment with a different photoresist mask pattern (Figure 1c). This time, most of the sample surface was protected only except for a 25 μ m window overlapping with one of the Hall bar channel. The intention was to block the conducting path between the two interface contacts completely. This was later confirmed by the I-V measurement (Figure 1f, red) where the resistance between C1 and C2 became so large that it was beyond the measurement limit (> $T\Omega$).

Figure 2a and b show the AFM topography and electrostatic force microscopy (EFM)^{45,46} images simultaneously taken at the center of the Hall bar region after the first plasma treatment. Topographical difference between plasma exposed and as-grown regions was not obvious (Figure 2a). Though an 1 Å level height contrast can be seen in finer scans (Figure 2c, d), where terrace structures from around 4 Å thick LaAlO₃ monolayers are also visible. The marginally higher topography (~1 Å) in exposed area rules out any potential etching effects and instead is consistent with the surface adsorption of small atoms such as O or OH. Unlike the weak topographical differences, as-grown and plasma exposed areas can be clearly distinguished in EFM images (Figure 2b). During the EFM

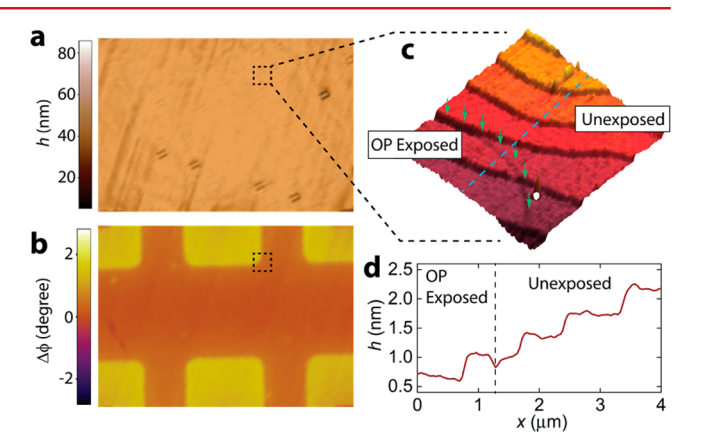


Figure 2. Surface topography and EFM profile after oxygen plasma exposure. (a) AFM topography and (b) EFM phase images of the 60 μ m \times 40 μ m region at the center of the hall bar. (c) AFM topography image zooming into the 4 μ m \times 4 μ m area marked by black dashed square in (a, b). Green arrows point to the boundary between protected and exposed regions. (d) Height profile along the blue dashed line as defined in (c).

imaging, the AFM tip was grounded and scanned at a lift height above the sample surface. An AC signal at the tip's resonant frequency was applied to the sample. Depending on the local surface potential, electrical conductivity, and permittivity, the electrostatic interaction between the tip and sample will vary and can be captured through the tip dither amplitude and phase (EFM signals). Because the EFM measurements were performed after days of air exposure and multiple solvent cleaning steps proceeding the oxygen plasma treatment, surface charging produced by plasma is expected to had already dissipated. The substantial contrast in EFM signal therefore points directly to the modifications of surface electronic states.

Kelvin probe force microscopy (KPFM)⁴⁷ was also performed to read out the surface potential and map the spatial resistivity changes. Figure 3b shows the surface potential measured before and after the second oxygen plasma treatment, where C1 and C2 were held at 2 V potential difference. Before

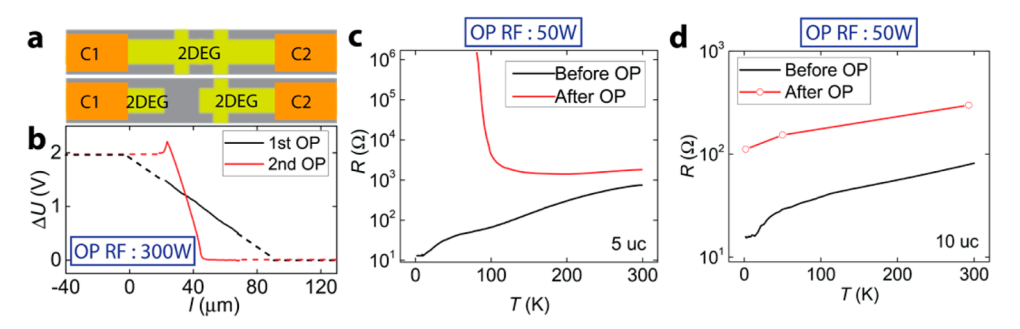


Figure 3. Tuning interface metallicity by controlling oxygen plasma dosage. (a) Illustrations of the interface 2DEG patterns and (b) KPFM surface potential between C1 and C2 after the first and second 1.5 min exposures to 300 W oxygen plasma. Solid lines in (b) represent the measurement data and dashed lines are extrapolations. (c, d) After 1 min exposure to 50 W oxygen plasma, (c) interface in 5-uc-LAO/STO was still conducting at room temperature but became insulating at low temperatures, and (d) interface in 10-uc-LAO/STO remained metallic in all temperatures but showed a large resistance increase.

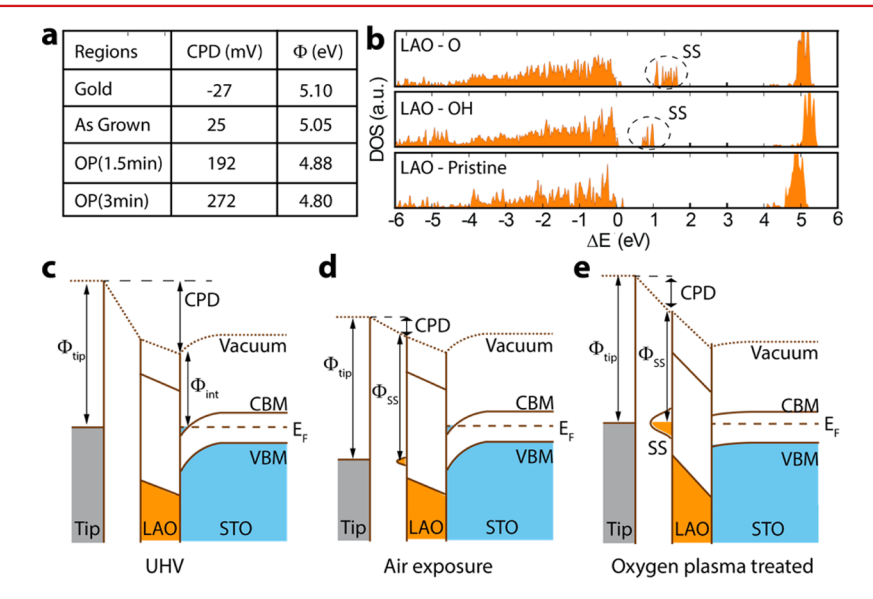


Figure 4. Oxygen related surface states and their effects on KPFM contact potential difference (CPD). (a) CPD and surface work functions (Φ) calibrated by gold reference. (b) Electron density of states (DOS) in the topmost LAO layer calculated for: O-terminated (top), OH-terminated (middle), and pristine (bottom) surface. (c) Without surface states, interface work function determines the CPD (CPD = $\Phi_{tip} - \Phi_{int}$). (d) When the surface states develop in air, CPD can instead be pinned by the surface states (CPD = $\Phi_{tip} - \Phi_{SS}$). (e) After oxygen plasma treatment, the increasing of surface states density as well as their filling level cause CPD to increase.

the second oxygen plasma treatment, potential varied linearly along the 90 μ m long channel, indicating a uniform resistivity distribution. Afterward, all 2 V dropped at once across the 25 μ m exposed window, showing unambiguously the local metal-to-insulator transition in the exposed region.

By controlling the oxygen plasma dosage, interface metallicity can be fine-tuned. A smaller dose of oxygen plasma (50W RF power for 1 min) was applied to unmasked 5 uc and 10 uc LAO/STO samples. Temperature dependent interface resistances were measured before and after the plasma treatment (Figure 3c, d). Prior to the exposure, both samples exhibited typical metallic characters. After the exposure, the 5 uc sample transited to an insulating character only at low temperatures (Figure 3c), whereas the 10 uc sample remained metallic but displayed a large resistance increase (Figure 3d). The altered electrical properties remained unchanged after months of air exposure and multiple solvent cleanings, indicating that the oxygen plasma induced surface modifications are long lasting.

From the perspective of polar catastrophe model, adding electronegative oxygens or hydroxyls to the surface should

enhance the polar field inside the LAO layer, which is expected to favor the interface doping rather than suppress it. To better understand the oxygen-plasma-induced interface metal-toinsulator transition, DFT calculations were performed. Figure 4b plots the electronic density of states (DOS) calculated for the topmost LAO layer with either pristine or O/OH terminated surfaces. The most obvious distinction is the development of in-gap surface states when the surface is O/OH terminated. Signatures of surface states can also be seen from KPFM measured surface potential. Without external bias, this signal represents the contact potential difference (CPD) that results from the different work functions of the AFM tip and the sample surface (CPD = Φ_{tip} – Φ_{sample}). Figure 4a lists the local CPD measured at surface regions that were never exposed to oxygen plasma (metallic) and regions exposed by different plasma dosages (insulating). Our CPD measurements in air exhibited values much smaller than in situ experiments performed in vacuum.⁴⁸ This is likely because, unlike samples with pristine surfaces where interface work function (Φ_{int}) dominates the CPD (Figure 4c), the development of in-gap surface states in air can effectively pin the Fermi level of the

probe (Figure 4d). It can also be seen that the interface metal-to-insulator transition induced by oxygen plasma is accompanied by an increasing CPD. This change reflects the increasing of the surface states density after oxygen plasma exposure and their raised electron filling level (Figure 4e).

Along with the creation of surface states, DFT results also showed that oxygen related surface adsorbates can strongly affect the interface doping when other electron-donating surface adsorbates are also present. Figure 5a plots the effective

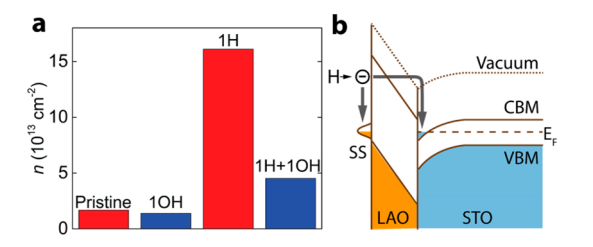


Figure 5. Oxygen surface states induced interface charge depletions. (a) Total densities of all conduction band states below Fermi level in the STO interface layers of Suc LaAlO₃/SrTiO₃. (b) Surface states created from oxygen adsorbates can accept electrons that will otherwise tunnel to the interfacial STO layers. Depending on the density of oxygen surface states, doping level at the interface will vary and lead to metal—insulator transitions.

doping density n of the five interfacial STO layers in a 5 uc LAO/STO heterostructure. n was calculated by integrating the total density of all conduction band states that are below the Fermi level. A relatively small amount of interface doping was found when the LAO surface is in its pristine state. Substantial increase of the doping level was found when hydrogens are introduced to the LAO surface. We note that hydrogens were considered here because they are the most abundant donor adsorbates that can form in the air. 49-54 Simply adding OH to pristine LAO surface does not have a major effect as can be appreciated in Figure 5. However, adding hydroxyls to H terminated surface leads to substantial reduction of n. This result indicates that direct charge transfer between the interface Ti d-orbitals and the oxygen surface states is likely not energetically favored. In contrast, possibly due to the strong electronegativity of oxygen and their spatial proximity, oxygen surface states can strongly trap electrons from other surface donors (Figure 5b).

The suppression of interface metallicity by oxygen plasma can therefore be explained by the following mechanism. When the density of surface electron-accepting states is low, assisted by the built-in field in the polar LAO layers, electrons from the electron-donating surface adsorbates can easily tunnel to the interface (Figure 5b). Such a charge transfer doping process will then lead to the interface metallicity. However, when the density of oxygen-related surface states is large, most electrons from the surface donors will instead be trapped in OH- or Oinduced acceptor-like surface states. As a result, electrons are depleted from LAO/STO interfaces after oxygen plasma treatment. The level of depletion can be tuned by the dosage of oxygen plasma and lead to different levels of electrical property changes as presented in Figure 3. The DFT calculation yields binding energy values of 5.0 and 3.6 eV for surface Al-OH and Al-O. Such strong bonding explains why the effect of oxygen plasma treatment is highly stable in atmosphere and robust against solvent cleanings.

In conclusion, an interfacial metal-to-insulator transition induced by oxygen plasma surface treatment was discovered in LAO/STO heterostructures. This effect can be understood by the competition for electrons between the surface states associated with oxygen adsorbates and the interface states related to Ti *d*-orbitals. Our results unambiguously showed the critical role of surface adsorptions in shaping the electronic properties of the LAO/STO interfaces. In addition, we also demonstrated that oxygen plasma treatment can be an effective and nondestructive method for patterning the LAO/STO interface 2DEG or controlling the local doping level. These capabilities are highly beneficial for the future electronic applications of complex oxide based low dimensional systems.

ASSOCIATED CONTENT

S Supporting Information

The Supporting Information is available free of charge on the ACS Publications website at DOI: 10.1021/acs.nanolett.6b00421.

Sample synthesis method, plasma treatment parameters, finite element simulation of interface conductance, and layer-resolved density of states generated from DFT calculations. (PDF)

AUTHOR INFORMATION

Corresponding Author

*E-mail: chcen@mail.wvu.edu.

Notes

The authors declare no competing financial interest.

ACKNOWLEDGMENTS

Experimental work at West Virginia University is supported by the Department of Energy Grant No. DE-SC-0010399 and National Science Foundation Grant No. NSF-1454950. Theoretical work acknowledge the support from the Extreme Science and Engineering Discovery Environment (XSEDE), which is supported by National Science Foundation Grant No. ACI-1053575. A.H.R. acknowledges the support of DMREF-NSF 1434897 and the Donors of the American Chemical Society Petroleum Research Fund for partial support of this research under contract 54075-ND10. Work at the University of Wisconsin was supported by funding from the DOE Office of Basic Energy Sciences under award number DE-FG02-06ER46327.

REFERENCES

- (1) Thiel, S.; Hammerl, G.; Schmehl, A.; Schneider, C. W.; Mannhart, J. Science 2006, 313, 1942–1945.
- (2) Reyren, N.; Thiel, S.; Caviglia, A. D.; Kourkoutis, L. F.; Hammerl, G.; Richter, C.; Schneider, C. W.; Kopp, T.; Rüetschi, A.-S.; Jaccard, D.; Gabay, M.; Muller, D. A.; Triscone, J.-M.; Mannhart, J. *Science* **2007**, 317, 1196–1199.
- (3) Caviglia, A. D.; Gariglio, S.; Reyren, N.; Jaccard, D.; Schneider, T.; Gabay, M.; Thiel, S.; Hammerl, G.; Mannhart, J.; Triscone, J. M. *Nature* **2008**, *456*, 624–627.
- (4) Gariglio, S.; Reyren, N.; Caviglia, A. D.; Triscone, J. M. J. Phys.: Condens. Matter 2009, 21, 164213.
- (5) Cheng, G.; Tomczyk, M.; Lu, S.; Veazey, J. P.; Huang, M.; Irvin, P.; Ryu, S.; Lee, H.; Eom, C.-B.; Hellberg, C. S.; Levy, J. *Nature* **2015**, 521, 196–199.
- (6) Kalisky, B.; Bert, J. A.; Klopfer, B. B.; Bell, C.; Sato, H. K.; Hosoda, M.; Hikita, Y.; Hwang, H. Y.; Moler, K. A. *Nat. Commun.* **2012**, *3*, 922.

(7) Bert, J. A.; Kalisky, B.; Bell, C.; Kim, M.; Hikita, Y.; Hwang, H. Y.; Moler, K. A. *Nat. Phys.* **2011**, *7*, 767–771.

- (8) Ariando; Wang, X.; Baskaran, G.; Liu, Z. Q.; Huijben, J.; Yi, J. B.; Annadi, A.; Barman, A. R.; Rusydi, A.; Dhar, S.; Feng, Y. P.; Ding, J.; Hilgenkamp, H.; Venkatesan, T. *Nat. Commun.* **2011**, *2*, 188.
- (9) Brinkman, A.; Huijben, M.; van Zalk, M.; Huijben, J.; Zeitler, U.; Maan, J. C.; van der Wiel, W. G.; Rijnders, G.; Blank, D. H. A.; Hilgenkamp, H. *Nat. Mater.* **2007**, *6*, 493–496.
- (10) Bi, F.; Huang, M.; Ryu, S.; Lee, H.; Bark, C.-W.; Eom, C.-B.; Irvin, P.; Levy, J. Nat. Commun. 2014, 5, 5019.
- (11) Irvin, P.; Ma, Y.; Bogorin, D. F.; Cen, C.; Bark, C. W.; Folkman, C. M.; Eom, C.-B.; Levy, J. Nat. Photonics 2010, 4, 849–852.
- (12) Tebano, A.; Fabbri, E.; Pergolesi, D.; Balestrino, G.; Traversa, E. ACS Nano **2012**, *6*, 1278–1283.
- (13) Rastogi, A.; Pulikkotil, J. J.; Auluck, S.; Hossain, Z.; Budhani, R. C. Phys. Rev. B: Condens. Matter Mater. Phys. 2012, 86, 075127.
- (14) Ma, Y.; Huang, M.; Ryu, S.; Bark, C. W.; Eom, C.-B.; Irvin, P.; Levy, J. Nano Lett. **2013**, *13*, 2884–2888.
- (15) Ohtomo, A.; Hwang, H. Y. Nature 2004, 427, 423-426.
- (16) Ohtomo, A.; Hwang, H. Y. Nature 2006, 441, 120-120.
- (17) Lee, J.; Demkov, A. A. Phys. Rev. B: Condens. Matter Mater. Phys. 2008, 78, 193104.
- (18) Nakagawa, N.; Hwang, H. Y.; Muller, D. A. Nat. Mater. 2006, 5, 204–209.
- (19) Zhong, Z.; Xu, P. X.; Kelly, P. J. Phys. Rev. B: Condens. Matter Mater. Phys. 2010, 82, 65127.
- (20) Liu, Z. Q.; Li, C. J.; Lü, W. M.; Huang, X. H.; Huang, Z.; Zeng, S. W.; Qiu, X. P.; Huang, L. S.; Annadi, A.; Chen, J. S.; Coey, J. M. D.; Venkatesan, T.; Ariando. *Phys. Rev. X* **2013**, *3*, 021010.
- (21) Kalabukhov, A. S.; Boikov, Y. A.; Serenkov, I. T.; Sakharov, V. I.; Popok, V. N.; Gunnarsson, R.; Börjesson, J.; Ljustina, N.; Olsson, E.; Winkler, D.; Claeson, T. *Phys. Rev. Lett.* **2009**, *103*, 146101.
- (22) Chambers, S. A.; Engelhard, M. H.; Shutthanandan, V.; Zhu, Z.; Droubay, T. C.; Qiao, L.; Sushko, P. V.; Feng, T.; Lee, H. D.; Gustafsson, T.; Garfunkel, E.; Shah, A. B.; Zuo, J. M.; Ramasse, Q. M. Surf. Sci. Rep. 2010, 65, 317–352.
- (23) Bark, C. W.; Felker, D. A.; Wang, Y.; Zhang, Y.; Jang, H. W.; Folkman, C. M.; Park, J. W.; Baek, S. H.; Zhou, H.; Fong, D. D.; Pan, X. Q.; Tsymbal, E. Y.; Rzchowski, M. S.; Eom, C. B. *Proc. Natl. Acad. Sci. U. S. A.* 2011, 108, 4720–4724.
- (24) Janotti, A.; Bjaalie, L.; Gordon, L.; Van de Walle, C. G. Phys. Rev. B: Condens. Matter Mater. Phys. 2012, 86, 241108.
- (25) Popović, Z. S.; Satpathy, S.; Martin, R. M. Phys. Rev. Lett. 2008, 101, 256801.
- (26) Copie, O.; Garcia, V.; Bödefeld, C.; Carrétéro, C.; Bibes, M.; Herranz, G.; Jacquet, E.; Maurice, J. L.; Vinter, B.; Fusil, S.; Bouzehouane, K.; Jaffrès, H.; Barthélémy, A. *Phys. Rev. Lett.* **2009**, *102*, 216804.
- (27) Huijben, M.; Koster, G.; Kruize, M. K.; Wenderich, S.; Verbeeck, J.; Bals, S.; Slooten, E.; Shi, B.; Molegraaf, H. J. A.; Kleibeuker, J. E.; van Aert, S.; Goedkoop, J. B.; Brinkman, A.; Blank, D. H. A.; Golden, M. S.; van Tendeloo, G.; Hilgenkamp, H.; Rijnders, G. Adv. Funct. Mater. 2013, 23, 5240–5248.
- (28) Shi, Y. J.; Wang, S.; Zhou, Y.; Ding, H. F.; Wu, D. Appl. Phys. Lett. 2013, 102, 071605.
- (29) Pentcheva, R.; Huijben, M.; Otte, K.; Pickett, W. E.; Kleibeuker, J. E.; Huijben, J.; Boschker, H.; Kockmann, D.; Siemons, W.; Koster, G.; Zandvliet, H. J. W.; Rijnders, G.; Blank, D. H. A.; Hilgenkamp, H.; Brinkman, A. *Phys. Rev. Lett.* **2010**, *104*, 166804.
- (30) Lesne, E.; Reyren, N.; Doennig, D.; Mattana, R.; Jaffrès, H.; Cros, V.; Petroff, F.; Choueikani, F.; Ohresser, P.; Pentcheva, R.; Barthélémy, A.; Bibes, M. *Nat. Commun.* **2014**, *5*, 4291.
- (31) Pentcheva, R.; Arras, R.; Otte, K.; Ruiz, V. G.; Pickett, W. E. *Philos. Trans. R. Soc., A* **2012**, *370*, 4904–4926.
- (32) Cen, C.; Thiel, S.; Mannhart, J.; Levy, J. Science 2009, 323, 1026-1030.
- (33) Cen, C.; Thiel, S.; Hammerl, G.; Schneider, C. W.; Andersen, K. E.; Hellberg, C. S.; Mannhart, J.; Levy, J. *Nat. Mater.* **2008**, *7*, 298–302.

- (34) Cheng, G.; Veazey, J. P.; Irvin, P.; Cen, C.; Bogorin, D. F.; Bi, F.; Huang, M.; Lu, S.; Bark, C.-W.; Ryu, S.; Cho, K.-H.; Eom, C.-B.; Levy, J. *Phys. Rev. X* **2013**, *3*, 011021.
- (35) Cheng, G.; Siles, P. F.; Bi, F.; Cen, C.; Bogorin, D. F.; Bark, C. W.; Folkman, C. M.; Park, J.-W.; Eom, C.-B.; Medeiros-Ribeiro, G.; Levy, J. Nat. Nanotechnol. 2011, 6, 343–347.
- (36) Schneider, C. W.; Thiel, S.; Hammerl, G.; Richter, C.; Mannhart, J. Appl. Phys. Lett. **2006**, 89, 122101.
- (37) Trier, F.; Prawiroatmodjo, G. E. D. K.; von Soosten, M.; Christensen, D. V.; Jespersen, T. S.; Chen, Y. Z.; Pryds, N. *Appl. Phys. Lett.* **2015**, *107*, 191604.
- (38) Banerjee, N.; Huijben, M.; Koster, G.; Rijnders, G. Appl. Phys. Lett. 2012, 100, 041601.
- (39) Lu, D.; Wu, Y.; Guo, J.; Lu, G.; Wang, Y.; Shen, J. Mater. Sci. Eng., B 2003, 97, 141–144.
- (40) Atanasova, E. D.; Kirov, K. I.; Kantardjeva, E. I. *Phys. Status Solidi A* **1981**, *64*, 73–80.
- (41) Lee, K. H.; Jang, H. W.; Kim, K.-B.; Tak, Y.-H.; Lee, J.-L. *J. Appl. Phys.* **2004**, *95*, 586–590.
- (42) Hollahan, J. R.; Carlson, G. L. J. Appl. Polym. Sci. 1970, 14, 2499-2508.
- (43) Suni, T.; Henttinen, K.; Suni, I.; Mäkinen, J. J. Electrochem. Soc. 2002, 149, G348-G351.
- (44) Song, J.-W.; Nam, Y.-H.; Park, M.-J.; Shin, S.-M.; Wehrspohn, R. B.; Lee, J.-H. RSC Adv. **2015**, *5*, 39177–39181.
- (45) Kantorovich, L. N.; Livshits, A. I.; Stoneham, M. J. Phys.: Condens. Matter 2000, 12, 795-814.
- (46) Xu, S.; Arnsdorf, M. F. Proc. Natl. Acad. Sci. U. S. A. 1995, 92, 10384–10388.
- (47) Nonnenmacher, M.; O'Boyle, M. P.; Wickramasinghe, H. K. Appl. Phys. Lett. 1991, 58, 2921–2923.
- (48) Susaki, T.; Makishima, A.; Hosono, H. Phys. Rev. B: Condens. Matter Mater. Phys. 2011, 84, 115456.
- (49) Merte, L. R.; Peng, G.; Bechstein, R.; Rieboldt, F.; Farberow, C. A.; Grabow, L. C.; Kudernatsch, W.; Wendt, S.; Lægsgaard, E.; Mavrikakis, M.; Besenbacher, F. Science 2012, 336, 889–893.
- (50) Di Valentin, C.; Pacchioni, G.; Selloni, A. Phys. Rev. Lett. 2006, 97, 166803.
- (51) Wendt, S.; Matthiesen, J.; Schaub, R.; Vestergaard, E. K.; Lægsgaard, E.; Besenbacher, F.; Hammer, B. *Phys. Rev. Lett.* **2006**, *96*, 066107
- (52) Li, S.-C.; Zhang, Z.; Sheppard, D.; Kay, B. D.; White, J. M.; Du, Y.; Lyubinetsky, I.; Henkelman, G.; Dohnálek, Z. *J. Am. Chem. Soc.* **2008**, *130*, 9080–9088.
- (53) Bi, F.; Bogorin, D. F.; Cen, C.; Bark, C. W.; Park, J.-W.; Eom, C.-B.; Levy, J. *Appl. Phys. Lett.* **2010**, *97*, 173110.
- (54) Fongkaew, I.; Limpijumnnong, S.; Lambrecht, W. R. L. Phys. Rev. B: Condens. Matter Mater. Phys. 2015, 92, 155416.